Biophysical Journal Volume 107 December 2014 2652–2661

Article

Self-Organizing Actomyosin Patterns on the Cell Cortex at Epithelial Cell-Cell Junctions

Thomas Moore,[1] Selwin K. Wu,[2] Magdalene Michael,[2] Alpha S. Yap,[2] Guillermo A. Gomez,[2] and Zoltan Neufeld[1,*]
[1]School of Mathematics and Physics and [2]Division of Molecular Cell Biology, Institute for Molecular Bioscience, The University of Queensland, Brisbane, Australia

ABSTRACT The behavior of actomyosin critically determines morphologically distinct patterns of contractility found at the interface between adherent cells. One such pattern is found at the apical region (zonula adherens) of cell-cell junctions in epithelia, where clusters of the adhesion molecule E-cadherin concentrate in a static pattern. Meanwhile, E-cadherin clusters throughout lateral cell-cell contacts display dynamic movements in the plane of the junctions. To gain insight into the principles that determine the nature and organization of these dynamic structures, we analyze this behavior by modeling the 2D actomyosin cell cortex as an active fluid medium. The numerical simulations show that the stability of the actin filaments influences the spatial structure and dynamics of the system. We find that in addition to static Turing-type patterns, persistent dynamic behavior occurs in a wide range of parameters. In the 2D model, mechanical stress-dependent actin breakdown is shown to produce a continuously changing network of actin bridges, whereas with a constant breakdown rate, more isolated clusters of actomyosin tend to form. The model qualitatively reproduces the dynamic and stable patterns experimentally observed at the junctions between epithelial cells.

INTRODUCTION

Understanding the mechanisms responsible for the formation of spatial patterns is a fundamental problem in biology. Significant progress in this field was made after the theory of Turing instability in nonlinear reaction-diffusion systems was developed (1). According to this theory, diffusive transport can generate spatial patterns in the presence of short-range positive feedback combined with long-range inhibition through fast-diffusing molecules (2,3). Recently, experiments have shown that the Turing mechanism plays a key role in developmental processes such as the patterning of feathers, formation of digits and hair follicles, and animal pigmentation (4,5). Reaction-diffusion-type mechanisms have also been found to contribute to intracellular concentration patterns and to be involved in the regulation of cell division and cell polarization (6–9).

Recent research has also highlighted the essential role that can be played by active mechanical forces and directed transport by advective flows, which can complement biochemical and genetic regulation and thus contribute to the formation of spatial structures in cells and tissues (10–12). In addition to muscle contraction and cell locomotion, mechanical interactions transmit signals that can influence cell behaviors such as growth, differentiation, polarization, and morphogenesis (13).

The mechanical properties of eukaryotic cells are mainly determined by the actin cytoskeleton and the cell cortex, which is composed of actin filaments, myosin, and other regulatory proteins that together generate contractile forces (14). The mesoscale behavior of this actomyosin system can be represented as a continuous medium of fluid or gel (15,16) in which internal contractile stresses are generated depending on the local protein concentrations. Hydrodynamic models governed by partial differential equations have been successfully applied to a diverse range of biological systems, including protrusions in moving keratocytes (17–19) and the formation of the contractile ring during cell division (20).

The interaction of actin and myosin can also lead to spontaneous pattern formation on the cell cortex. Propagating wave-like patterns of actin polymerization have been observed in migrating cells (e.g., neutrophils), which play a role in regulating motility and chemotaxis through the formation of protrusions (21,22). Another example was recently identified at the adhesive junctions between simple polarized epithelial cells (23). These junctions are formed by the cell adhesion receptor E-cadherin, which distributes as clusters both in a 1D apical ring (known as the zonula adherens (ZA)) and throughout the 2D lateral surface immediately subjacent to the ZA (the lateral adherens junction (LAJ)) (23). Cadherin clusters at both the ZA and the lateral junctions associate with the actomyosin cortex. However, live-cell imaging of these E-cadherin clusters revealed different patterns of planar motion within these junctions. The ZA displayed a relatively static pattern consisting of multiple stationary clusters of cadherin. In contrast, the LAJ was distinguished by dynamic behavior, which

Submitted July 8, 2014, and accepted for publication October 28, 2014.
*Correspondence: z.neufeld@uq.edu.au
Editor: Leah Edelstein-Keshet.

0006-3495/14/12/2652/10 $2.00
http://dx.doi.org/10.1016/j.bpj.2014.10.045

typically involved clusters moving and merging, and new ones forming spontaneously. The qualitative behavior of these patterns of cadherin cluster movement appeared to reflect differences in the organization and distribution of mechanical stresses within the actomyosin cortex that was coupled to cadherin clusters. Stress could be sustained at the ZA but was rapidly dissipated at the LAJ, a difference that reflected differences in F-actin stability at these two locations. At a physiological level, these patterns of mechanical tension at the junctions exerted a morphogenetic influence that integrated cells into the epithelia, preventing them from being extruded (23).

To better understand how the actomyosin cortex could generate these distinct patterns of E-cadherin cluster movement and their associated dynamic patterns of stress, we sought to apply active fluid theory to describe junctional motion. The spontaneous formation of actomyosin patterns in a simple active fluid model was reported by Bois et al. (24), but that model was restricted to one dimension and the only pattern observed was a single, stable peak of high protein concentration, rather than the dynamic patterns that were observed experimentally at cadherin junctions (23). Here, we demonstrate that a simple natural extension to this model allows the qualitative reproduction of the various stable and dynamic actomyosin patterns observed experimentally, in both one and two dimensions. We also study the role of the stress dependence of the stability of actin filaments in the distribution of actomyosin.

MATERIALS AND METHODS

Cell culture

Caco-2 cells were cultured in RPMI media supplemented with 10% fetal bovine serum, 1% nonessential amino acids, 1% L-glutamine, and 1% Pen/Strep. For live-cell imaging, cells were grown on 29 mm glass-bottom dishes (Shengyou Biotechnology, China) and incubated in phenol-red-free Hank's balanced salt solution supplemented with 5% fetal bovine serum, 10 mM HEPES (pH 7.4), and 5 mM $CaCl_2$. Fully confluent cultures were used for all experiments.

Plasmids and lentivirus

The lentivirus expression vector LentiLox pLL5.0 (backbone pLL3.7) and the third-generation packaging constructs pMDLg/pRRE, RSV-Rev, and pMD.G were gifts from Jim Bear (University of North Carolina at Chapel Hill). The calponin homology domain of Utrophin fused to GFP(GFP-UtrCH) binds to F-actin and its intensity at the cortex provides a relative estimate of F-actin content (25). pLL5.0 GFP-UtrCH was generated by subcloning GFP-UtrCH (a gift from Bill Bement, University of Wisconsin) into BamHI/SbfI sites of the pLL5.0 construct. For expression of constructs, cells were transduced with recombinant lentivirus at 30% confluency with polybrene for 24 h and split for experiments after another 20 h.

Inhibitors

Latrunculin-A (1 μM; Sigma-Aldrich) and jasplakinolide (0.2 μM; Merck) were applied to Caco-2 monolayers 15–30 min before imaging.

Live-cell microscopy

Wide-field microscopy was performed on a Personal Deltavision deconvolution microscope with a Roper Coolsnap HQ2 monochrome camera (Applied Precision) 60×, 1.42 NA, with PlanApo objectives (Olympus, Japan). Time-lapse images were acquired as 10–40 z stacks (0.2 μm z step) and deconvolved using the DeltaVision software (Applied Precision). The exposure time (0.1 s per z stack), gain, and level of the transmission light (15%) were kept constant for all live-cell-imaging experiments.

Image processing and analysis

The images were processed with ImageJ (http://rsb.info.nih.gov/ij/). A rolling ball (5 pixels) background subtraction and median filter of one pixel radius were sequentially applied on the original z stacks, which were then z projected as a sum of slices (see Fig. 7 *a*). For the movies presented, effects of photobleaching were corrected using the Simple Ratio Method of the Bleach Correction ImageJ plugin by K. Miura and J. Rietdorf (EMBL Heidelberg). The bit rate of all images presented was adjusted to 8 bits. To ensure consistent contrast for all images, the minimum intensity values were all set to 25 and the maximum intensity value was adjusted to 180. Further details of the experimental methods are also described in Wu et al. (23).

Particle image velocitometry (PIV) was performed on regions of interest of 100 × 100 pixels cropped from GFP-Utrophin movies at the lateral cortex and analyzed in MATLAB (The MathWorks, Natick, MA) using OPEN PIV script (http://www.openpiv.net/) with an interrogation window size = 16, spacing/overlap = 8, S/N type 2, outlier filter = 100, and jump = 1 (27).

RESULTS

Mathematical model

F-actin polymers associate with myosin molecules to form an active fluid in which the contractile stress can be described as an increasing function of the local density of the component proteins. The active stress induces a flow in the medium and this active transport in turn affects the distribution of actin and myosin, and potentially also other proteins that are associated with them.

For simplicity, we first consider the case of a 1D domain, and later we discuss the extension to two dimensions. The 1D domain may be envisaged to correspond to the 1D ring of the ZA in epithelial cells. Following Bois et al. (24), the dynamics of the system can be described by the equations

$$\partial_x(\eta\partial_x v + \zeta f(C)) = \gamma v$$

$$\partial_t C + \partial_x(vC) = D\partial_x^2 C + S - dC. \qquad (1)$$

The first equation represents the balance between friction and the divergence of viscous and active stresses. The viscosity η is assumed to be constant and the active stress is a hyperbolic function $f(C) = C/(C + \kappa)$ of the F-actin concentration $C(x,t)$ with half-saturation constant κ. The second equation describes advection and diffusion of F-actin, and we also included on the right-hand side the turnover of F-actin resulting from the polymerization of actin monomers at rate S and the breakup of F-actin filaments with

an average characteristic lifetime $1/d$. Later, we also consider the case of stress-dependent breakdown of the actin filaments, which has consequences for pattern formation in two dimensions.

A separate myosin species is not directly incorporated into this model. In reality, activated myosin exists in two states: it can be bound to actin, enabling actin contraction, or it can be an unbound and inactive in the cytosol. What is important is the dynamics of myosin that is bound to actin. Consider two extremes: First, when myosin rapidly attaches and detaches from actin, and free myosin rapidly diffuses when it is unattached, the amount of myosin that can exert active stress is proportional to the amount of actin that is present. In the other limit, the myosin never detaches and is always bound to actin, in which case its dynamics exactly mirror those of actin. In either case, because actin is the scaffold for active stress to be transmitted and is itself transported, myosin's contribution to active stresses is not really distinguishable from that of actin. Because of this co-accumulation, which was also confirmed experimentally (23,28), to a reasonable approximation we can model the movement of actomyosin as a single component.

Introducing the length-scale unit $l = (\eta/\gamma)^{1/2}$ and velocity scale $U = \zeta/(\eta\gamma)^{1/2}$, the above system can be rewritten in a nondimensional form as

$$\partial_x^2 v + \partial_x f(c) = v,$$

$$\partial_t c + Pe\,\partial_x(vc) = \partial_x^2 c + s - \alpha c. \tag{2}$$

where $Pe = Ul/D = \zeta/D\gamma$ is the Peclet number (i.e., a measure of the relative strength of directed active transport versus random diffusion), $c = C/\kappa$ is the nondimensional concentration, and using the timescale unit $\tau = \eta D/\gamma$, the rescaled parameters are $s = S/\kappa\tau$ and $\alpha = d/\tau$.

Stability analysis

When the source and consumption terms are ignored, i.e., $s = \alpha = 0$, the total F-actin is conserved. For this case, it was previously shown that either the concentration of actin is uniform and no flow is induced ($v = 0$) or there is a stable peak of high actin density sustained by a convergent flow, with the inward flux balanced by diffusion away from the concentrated peak (24). For sufficiently large systems, multiple peaks may form initially and then gradually merge into a single peak, although in large systems this may be a very slow process since the interaction between well-separated peaks is weak.

The boundary of the parameter regions corresponding to uniform steady states or stable peaks can be determined from a linear stability analysis. Consider a small perturbation around the uniform steady state of the form $v = \delta v_0\, e^{\beta t} e^{ikx}$, $c = c_0 + \delta c_0\, e^{\beta t} e^{ikx}$ with wavenumber $k_n = 2\pi n/L$, $n = 1,2,\ldots$ (corresponding to periodic boundary conditions; choose $k_n = \pi n/L$ for a no-flux condition instead). Since the amplitude of the perturbation is small, we can linearize the system (Eq. 2) and obtain

$$-k^2\delta v_0 + ikf'(c_0)\delta c_0 = \delta v_0$$

$$\beta\,\delta c_0 + ikPec_0\delta v_0 = -k^2\delta c_0. \tag{3}$$

Eliminating the amplitudes δv_0 and δc_0, the growth rate of the perturbation with wavenumber k can be expressed as

$$\beta(k) = -k^2\left(1 - Pe\frac{c_0}{(1+k^2)(1+c_0)^2}\right).$$

The uniform steady state is unstable and patterns spontaneously form when the growth rate is positive for some k. Thus, the condition of the pattern-forming instability on periodic domain is that

$$Pe > \left(1 + \frac{4\pi^2}{L^2}\right)\frac{(1+c_0)^2}{c_0},$$

where L is the domain length and c_0 is the uniform steady-state concentration. In the limit of a large domain size compared with the characteristic wavelength of the instability, the necessary condition becomes

$$Pe > \frac{(1+c_0)^2}{c_0}.$$

When the source-consumption term is added to the model (α, $s > 0$) the uniform steady state is $c_0 = s/\alpha$ and the dispersion relation is modified to

$$\beta(k) = -k^2\left(1 - Pe\frac{c_0}{(1+k^2)(1+c_0)^2}\right) - \alpha.$$

The maximum growth rate is obtained when $\beta'(k) = 0$ corresponding to the wavenumber

$$k_0 = \left(\frac{\sqrt{Pec_0}}{1+c_0} - 1\right)^{1/2}.$$

Substituting back into the dispersion relation, we obtain

$$\left(\frac{\sqrt{Pec_0}}{1+c_0} - 1\right)^2 > \alpha,$$

and the condition for pattern formation becomes

$$Pe > \left(1 + \sqrt{\alpha}\right)^2\frac{(1+c_0)^2}{c_0}, \tag{4}$$

assuming that the wavenumber k_0 is permitted by the boundary conditions (e.g., when $L >> k_0$).

Numerical results

When the above condition is satisfied, the patterns that form can be studied numerically. We found that F-actin turnover has two main effects. First, when the uniform system is unstable and peaks of high concentration form, these growing multipeak solutions are stabilized without merging (Figs. 1 and 2). Second, for a certain range of parameters, the actin concentration field does not reach a static distribution, but a dynamical state is maintained either in the form of moving, oscillating peaks that nevertheless preserve their identity or in a system of continuously merging peaks accompanied by the formation of new ones in the vacant space created between them. A typical example is shown in Fig. 3.

The phase diagram of the 1D system indicates different types of behavior: uniform or static and dynamic patterns (Fig. 4). The boundary between uniform and nonuniform solutions is in agreement with the linear stability analysis (Eq. 4). The regions of dynamic behavior (*blue* in Fig. 4) have a band-like structure separating regions of stable nonuniform patterns (*green*) corresponding to different numbers of stable peaks. In these bands, the ratio of the domain size to the pattern's wavelength is not sufficiently close to an integer; therefore, the system cannot settle into one of the stable solutions, so it moves around dynamically. For example, the stripe of dynamic behavior at low c_0 and high Pe separates the region in which one peak forms from the region with two static peaks. Along this stripe, when two peaks form, the distance between them is shorter than in the case of static peaks and therefore they gradually merge, leaving behind a sufficiently large uniform region for the instability to form a new peak of concentrated actin. In the same way, a thicker band of dynamic behavior separates the regions with two and three stable peaks. However, we also see that for a sufficiently high Peclet number and F-actin concentration, we have large connected regions where the system does not stabilize. In these regions, the dynamic patterns are robust and the qualitative behavior is not sensitive to the values of the parameters.

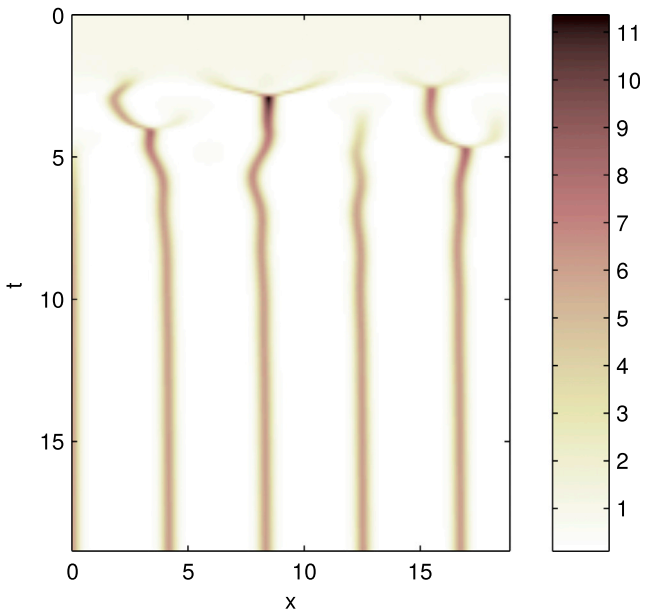

FIGURE 1 Space-time plot of actin concentration from numerical simulation of the 1D model with no-flux boundary conditions ($\partial_x c(x=0, L)=0$, $v(x=0, L)=0$), showing actin concentrated into multiple clusters. The model parameters are $Pe=50$, $c_0=1$, $\alpha=1$, $L=8\pi$. To see this figure in color, go online.

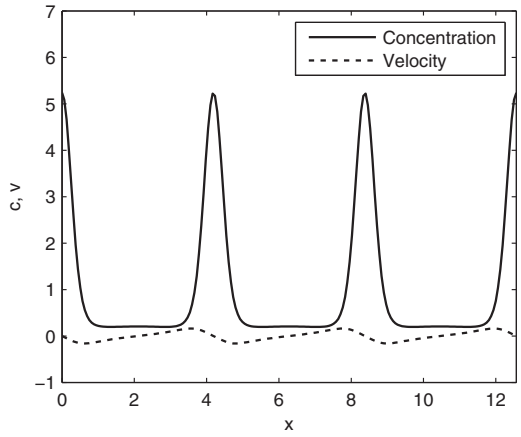

FIGURE 2 Stable steady-state solution of the 1D model: actin concentration and velocity. Parameters: $Pe=40$, $\alpha=1$, $c_0=1$, $L=4\pi$. Boundary conditions: $\partial_x c(x=0, L)=0$, $v(x=0, L)=0$.

Extension of the model to two dimensions

Apart from the ZA, the biological system of interest is a 2D surface along the interface between two cells corresponding

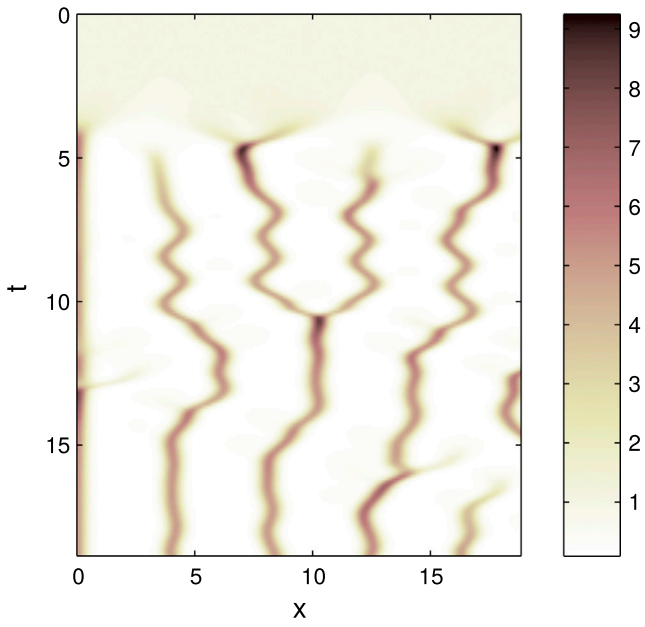

FIGURE 3 Dynamic pattern of moving and merging clusters of actin in the 1D model. Model parameters: $Pe=50$, $c_0=4$, $\alpha=1$, $L=8\pi$, with no-flux boundary conditions. To see this figure in color, go online.

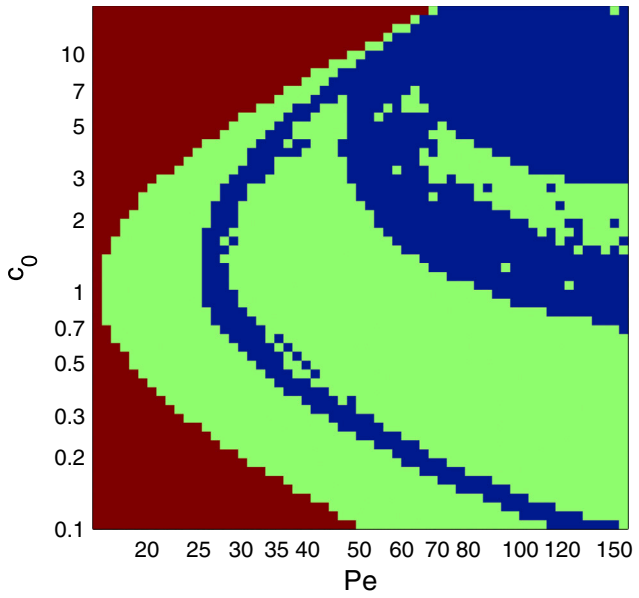

FIGURE 4 Numerically generated phase diagram of the 1D system with no-flux boundary conditions for $\alpha = 1$ and $L = 4\pi$. Red regions, uniform steady state; green, stable nonuniform patterns; blue, dynamic behavior. To see this figure in color, go online.

to the LAJ (see Fig. 7 *a*) (23,28). Therefore, we also studied the 2D version of the model. We consider the simplest generalization of the 1D case and neglect the polar nature of actin. The system is then described by the equations

$$\begin{aligned} \lambda\Delta\boldsymbol{v} + (1-\lambda)\nabla(\nabla\cdot\boldsymbol{v}) + \nabla f(c) &= \boldsymbol{v} \\ \partial_t c + Pe\nabla\cdot(c\boldsymbol{v}) &= \Delta c + s - \alpha c \end{aligned}, \qquad (5)$$

where the velocity field equation was slightly modified to account for the occurrence of both bulk and shear viscosities in higher-dimensional compressible flows. The relative magnitude of the two types of viscosity coefficients is determined by the nondimensional parameter $\lambda \in [0,1]$, which is defined as

$$\lambda = \frac{\eta}{\eta + \eta_v},$$

where η_v is the bulk viscosity. For a thin sheet made out of an incompressible fluid, $\lambda = 0.25$, and this value was used for all experiments (though we note that the system does not appear to be very sensitive to changes in λ).

The model described by Eq. 5 was solved numerically using a Lax-Friedrichs finite-difference scheme on a square domain with periodic boundary conditions. When the spatially uniform steady state is unstable, F-actin concentrates into clumps, forming a hexagonal lattice, with convergent isotropic flow around them (Fig. 5). For some parameters, the clumps connect to each other and develop into stripe patterns whose transverse profile is then equivalent to the 1D solution. These stationary patterns are similar to the well-known Turing patterns that develop in reaction-diffusion systems. However, in this case they do not arise from nonlinear reaction kinetics and differential diffusion, but rather from the coupling between the concentration field and the flow it generates. Examples of the development of the static patterns from random initial conditions are shown in Movies S1 and S2 in the Supporting Material.

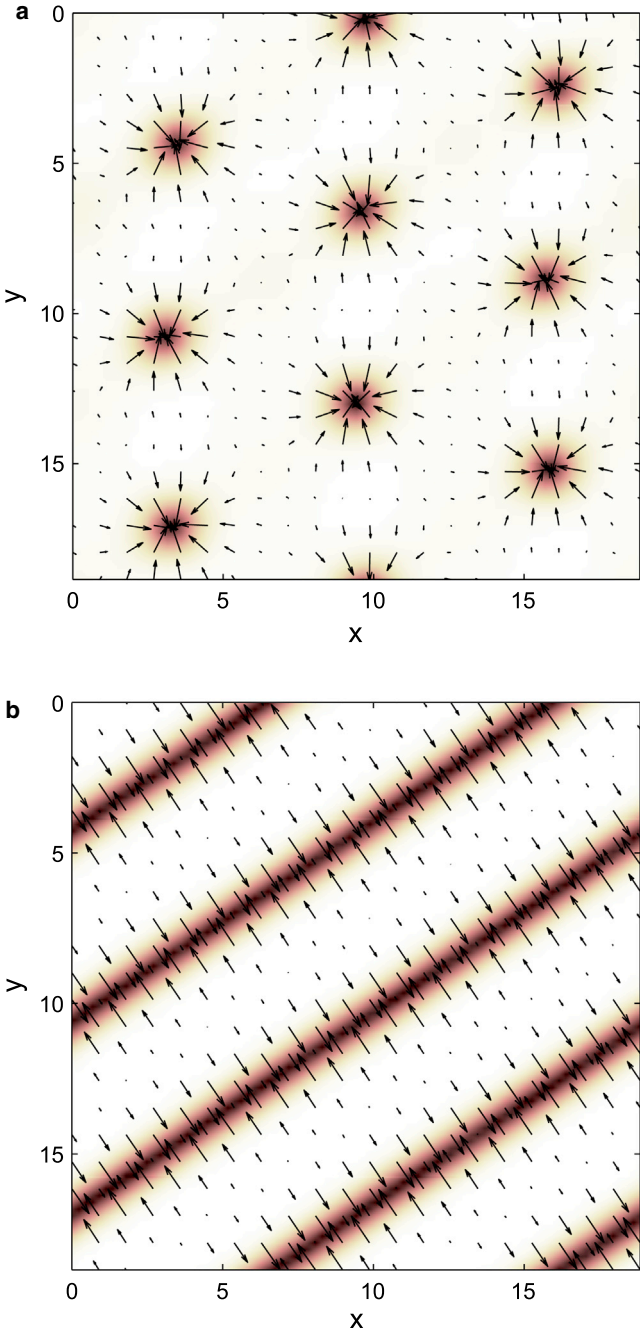

FIGURE 5 Stable spots and stripe patterns of concentrated F-actin in the 2D model solved numerically on a periodic domain $6\pi \times 6\pi$. Model parameters: $Pe = 25$, $\alpha = 1$, $\lambda = 0.25$, and $c_0 = 0.3$ (*top*), and $c_0 = 1.5$ (*bottom*). To see this figure in color, go online.

Although the Turing patterns in a nonmoving medium are always static, here, as in 1D, dynamically changing patterns

also arise when *Pe* is increased. In this regime the actin clumps (or stripes) continuously move, merge with other clusters, and form new clusters in formerly vacant regions (see Movie S3). The phase diagram obtained from numerical simulations varying *Pe* and $c_0 = s/\alpha$ shows that such dynamic behavior is prevalent for large *Pe* (Fig. 6). In making this phase diagram, we manually differentiated the static stripe and static spot patterns by looking at images of the final states of the systems. Whether a system was uniform static, nonuniform static, or behaved dynamically was determined automatically. Each system was run for 300 time units and over the last 5% of the simulation the average rate of change of concentration was measured. This rate was vanishingly small for static patterns, so it was a good indicator of whether or not the system was still moving dynamically.

Experimental manipulation of F-actin stability

To qualitatively compare these simulated structures with living cells, we examined the dynamic distribution of cortical F-actin in Caco-2 cells. To image F-actin in live-cell imaging, we expressed the F-actin-binding calponin-homology domain of utrophin fused to GFP (25). We took advantage of slanted cell-cell junctions that allowed us to image en face both the apical ZA and the LAJ (Fig. 7 *a*). Kymographs from junctions between control cells showed that the apical concentration of F-actin in the region of the ZA was relatively stable (Fig. 7 *b*), whereas the LAJ displayed cyclical condensation and disassembly of the F-actin network (see also Movie S4). To emulate the effect of reducing c_0 to very low levels, we disrupted F-actin integrity with Latrunculin-A (1 μM, 15 min), which blocks actin polymerization. We found that the F-actin networks disassembled at both the ZA and lateral junctions to form relatively static spots at the junctional cortex (Fig. 7, *middle row*). This change causing the breakup of the F-actin ring of the ZA is analogous to the transition from a uniform state with high tension to the formation of static clusters when the parameter c_0 is decreased in the model. Conversely, to mimic the effect of increasing c_0, we incubated cells for 30 min with 0.2 μM jasplakinolide, a drug that stabilizes F-actin filaments. This led to the immobilization of the F-actin network, causing it to condense into larger and more intense spots at the lateral junction. These structures may then contribute to increased tension as previously reported (23). In this case, the larger actin clusters may be interpreted as an intermediate stage in which a zone of high mechanical tension similar to the ZA partially extends into the lateral membrane.

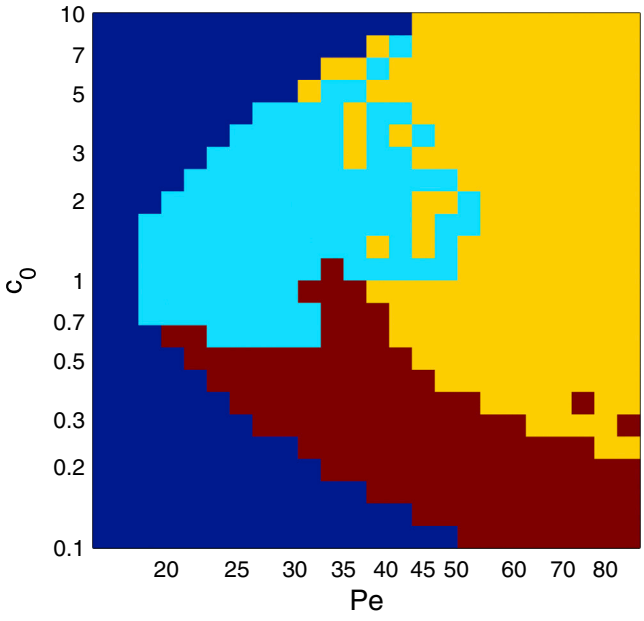

FIGURE 6 Phase diagram of the 2D system with periodic boundary conditions for $\alpha = 1$, $\lambda = 0.25$, and $L = 4\pi$. Initial condition: uniform concentration, c_0, with random noise. Blue regions, uniform steady state; cyan, static stripe patterns; red, spot patterns; orange, dynamic behavior. To see this figure in color, go online.

Experimental studies found that regulatory proteins may modulate the stability of actin filaments on the cell cortex. In particular, the protein N-WASP selectively localizes to the ZA, rather than to lateral junctions. There it is responsible for increasing F-actin stability in that apical region (23,29), contributing to the formation of a continuous ring of E-cadherin clusters and increased mechanical tension. This type of behavior is analogous to the stable uniform solution of the 1D model when the total equilibrium concentration of actin $c_0 = s/\alpha$ is sufficiently large, which is consistent with high actin stability (i.e., small α). To determine whether the spatial modulation of actin stability can also produce a localized continuous ring when embedded into a 2D dynamic pattern, we solved the system assuming that the actin decay rate is 10 times smaller in the central band $2L/5 < y < 3L/5$ than in the rest of the domain. As shown in Fig. 8 (see also Movie S5), the enhanced stability of actin in the central band leads to the formation of an approximately stationary, narrow ring of concentrated F-actin that coexists with the fluctuating dynamic behavior present in the rest of the domain.

The F-actin visualized experimentally at the LAJ appeared to form short cables (Fig. 7, *top panel*), which represent elongated bridges (23,28), instead of the clumps seen in the simulations. Therefore, we also explored whether simple modifications of the model could reproduce such patterns. A natural refinement is to assume that the stability of F-actin filaments is dependent on the active stress, so that the breakdown rate of actin increases with the actin concentration. Indeed, experimentally we observed that myosin II contributes to actin filament turnover at lateral junctions, as depletion of myosin II increased actin stability at these sites and reduced the active movements of actomyosin observed in cells (23). Thus, we set the decay term in

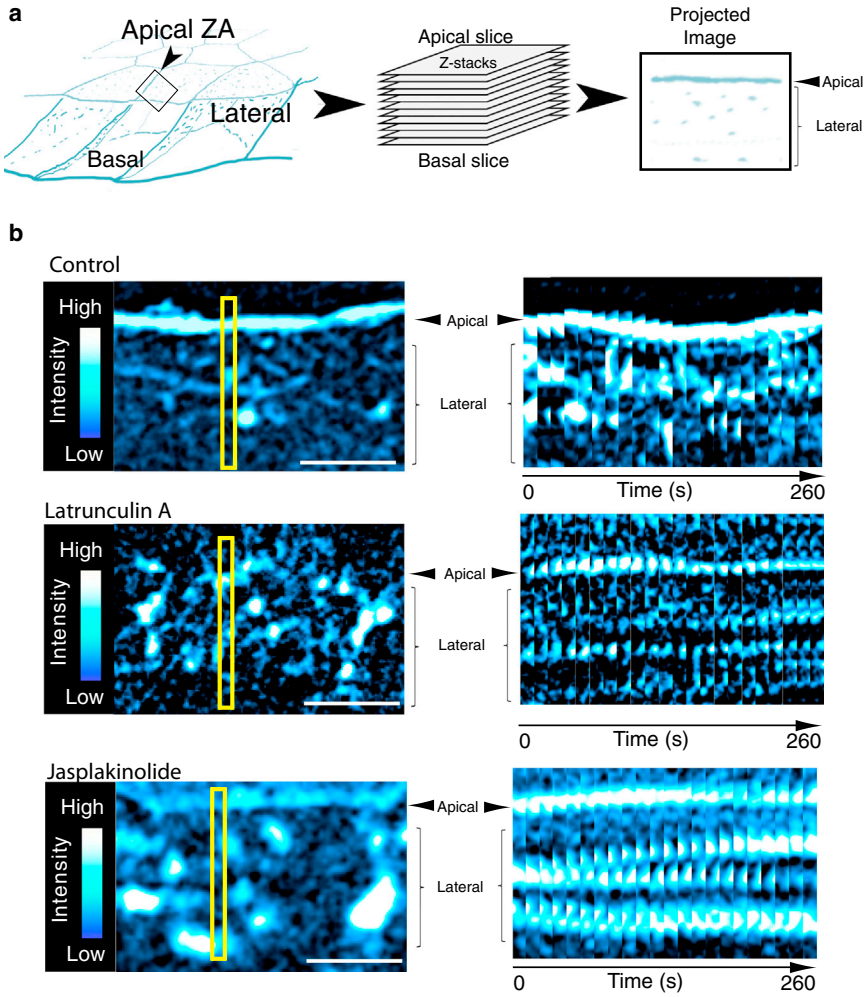

FIGURE 7 F-actin organization and dynamics at Caco-2 cell-cell junctions. (*a*) Workflow diagram illustrating 3D imaging of simple polarized epithelia, where individual z slices across a tilted junction are combined into a stack and then projected into a single image. (*b*) Representative images from time-lapse series of junctional F-actin (color coded with *hot cyan*) for control cells, latrunculin A-treated cells, or jasplakinolide-treated cells are shown in the left-hand panels. The corresponding intensity heatmaps of the images are on the far left. The F-actin fluorescence intensity levels reflect the relative levels of F-actin content. Lower F-actin intensity levels are color coded in blue, and white represents the area of high F-actin intensity. Kymographs of the areas indicated by yellow boxes in each of the left-hand panels are shown in the corresponding right-hand panels. Scale bars: 5 μm. To see this figure in color, go online.

the advection-diffusion equation to be a quadratic function of the actin concentration:

$$\partial_t c + Pe\nabla \cdot (c\boldsymbol{v}) = \Delta c + s - \alpha c^2, \tag{6}$$

and in this case,

$$c_0 = \sqrt{\frac{s}{\alpha}}. \tag{7}$$

With this modification, we find that actin typically condenses into a dynamic network of high actin concentration (Fig. 9; Movie S6). In this case, the ring-like actin structures contract and merge into a single patch while creating larger empty spaces around them where new patches emerge and form actin bridges that connect them to the rest of the network. The process repeats itself, producing a continuously changing network of actin. This simulation reproduced more closely the patterns of junctional actomyosin observed in cells (23,28).

To establish the relevance of the patterns observed in the model for the experimental system, we used PIV analysis of the actin flow on the cortex to obtain an order-of-magnitude estimate of the Peclet number. A region of interest of 100 × 100 pixels was cropped from GFP-Utrophin movies at the lateral cortex and analyzed in MATLAB using the OpenPIV software package (http://www.openpiv.net/). By tracking the field of inhomogeneities through the autocorrelation of three consecutive image frames, the PIV analysis generates a velocity field associated with the movement of actin within the cortex. We analyzed the obtained velocity fields using the spatial analysis toolbox for PIV (http://www.openpiv.net/openpiv-spatial-analysis-toolbox/) to calculate individual velocity displacements of actin cables. We then used these velocity values to compute the distribution of velocity values and their average values (Fig. 10).

Finally, to estimate the diffusivity of F-actin, we obtained velocity fields of actin cables using PIV as described above from cells depleted of myosin IIA by RNAi (myosin IIA KD) (23). We performed simulations of particle trajectories $r(t)$ using the obtained velocity fields by solving the equation $\dot{\boldsymbol{r}}(t) = \boldsymbol{v}(\boldsymbol{r}, t)$ numerically. Calculating the average dispersion rate for 5000 particles with random initial

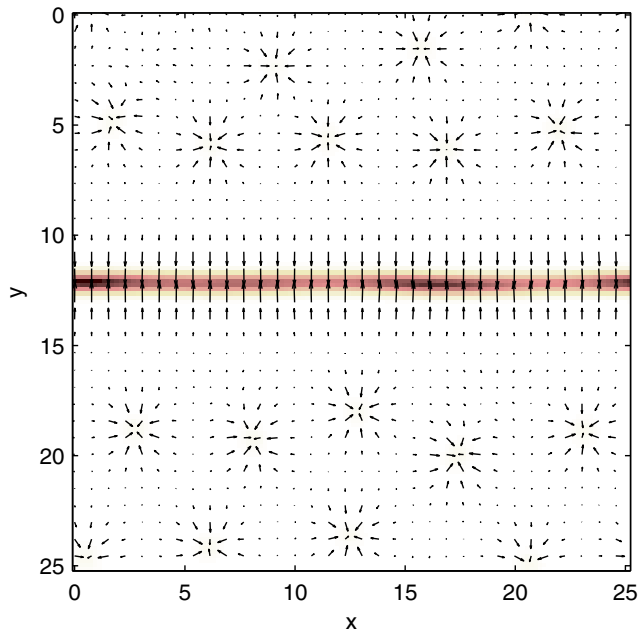

FIGURE 8 Snapshot of the F-actin concentration field from a simulation in which the decay rate of actin is lower in a central horizontal band of width $L/6$ ($\alpha = 0.1$), whereas in the rest of the system $\alpha = 1$. This simulation shows that dynamic clusters may coexist with the uniform state when the decay rate varies in space. The other parameters are $Pe = 55$, $c_0 = 0.5$, and $L = 8\pi$. To see this figure in color, go online.

positions using the relation $\langle(\boldsymbol{r_i}(t) - \boldsymbol{r_i}(0))^2\rangle \approx 4Dt$, we extracted the effective diffusion coefficient of F-actin: $D \approx 2 \times 10^{-4}$ μm^2/s.

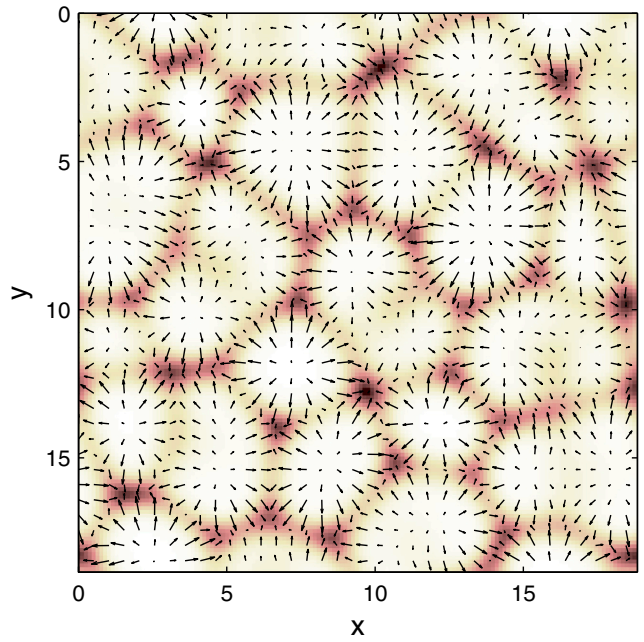

FIGURE 9 Snapshot of the dynamically moving, merging, and splitting peaks in the model with a concentration-dependent breakdown rate. $Pe = 55$, $\alpha = 1$, $c_0 = 2$, $\lambda = 0.25$, $L = 6\pi$. To see this figure in color, go online.

From these values and the typical distance between actin clusters, $L \approx 2$ μm, we can obtain an estimate of the order of magnitude of the Peclet number for the actin flow on the cortex as $Pe = UD/L \approx 30$. This value is roughly consistent with the region of the phase diagram where patterns may form. Furthermore, this region of the parameters also allows for modulation of the pattern-formation mechanism through the variation of c_0, which is dependent on actin stability.

DISCUSSION

The Turing mechanism for pattern formation based on the interplay between differential diffusion and nonlinear reaction kinetics in multicomponent systems is theoretically well understood and has been observed in experiments and various applications. Recent research in biological systems has also identified the essential role that mechanical interactions can play in complementing biochemical signals to regulate self-assembly and dynamic behavior in single cells or multicellular tissues. Mathematical models of chemomechanical systems have been shown to produce a range of behaviors and have been used to investigate certain cell behaviors.

We recently found that cortical zones with distinct patterns of actomyosin dynamics are established at the cell-cell junctions between epithelial cells. These generate different levels of contractile tension, even within the same junction, that are determined by F-actin stability (23). Motivated by these experimental observations, we investigated the range of dynamic behaviors that can be generated by a simple minimal model that takes into consideration active mechanical stress and the resulting flow in the medium. We now show that when the conservation of the contractile component is relaxed and is replaced by a dynamic equilibrium resulting from the presence of a source and decay, even a single-component system is capable of producing a rich variety of patterns. We note that the possibility of pulsatile actomyosin patterns was demonstrated recently by Kumar et al. (30) in a model that considered two species with different diffusivities or turnover rates.

In our model, the two key parameters that determine the spatial structures are the total concentration of actomyosin at the cortex (c_0) and the Peclet number that is inversely proportional to the drag coefficient. Thus, increased Pe corresponds to enhanced movement of the protein structures within the cortex. The average concentration c_0 is determined by the balance between the formation and decay of F-actin in the actomyosin contractile apparatus.

When Pe is low, the friction forces dominate and suppress the flow of actomyosin, and therefore spatial patterns cannot form. When Pe is larger than a certain threshold, whose value depends on actin stability (α), the organization of actomyosin is determined by the total concentration, c_0. If the actomyosin concentration is low, it generates weak tension and the distribution remains uniform. Similarly, in the

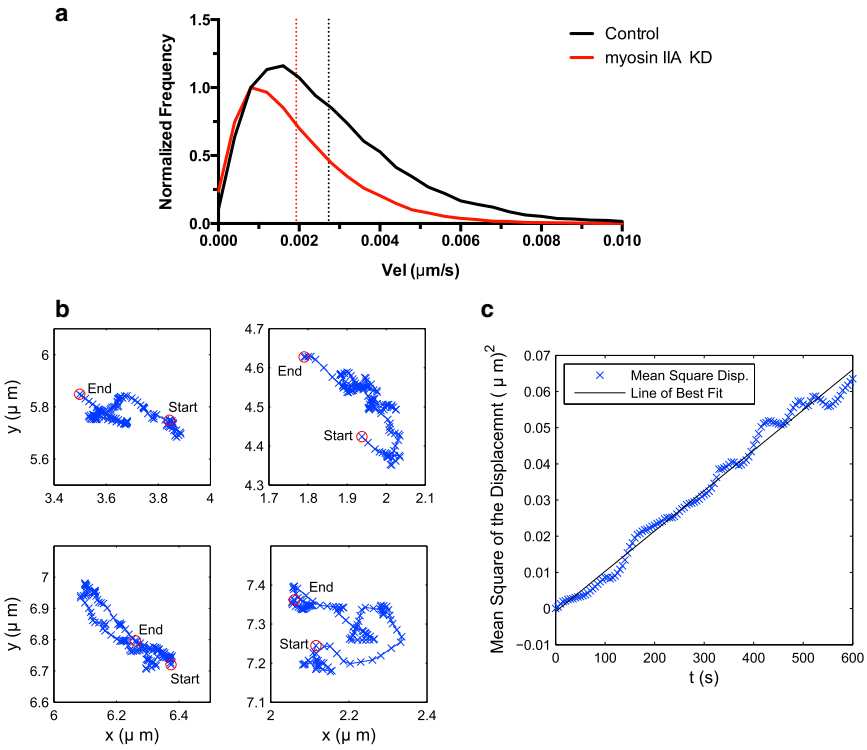

FIGURE 10 Top: velocity histograms obtained from the PIV analysis of actin flow. The average velocities are $U = 0.0027$ μm/s (Ctrl) and $U_{KD} = 0.0019$ μm/s for myosin IIA KD. Middle: examples of simulated particle trajectories calculated using the velocity field obtained from the PIV analysis of myosin IIA KD cells. Bottom: mean-square displacement $\langle(\boldsymbol{r_i}(t) - \boldsymbol{r_i}(0))^2\rangle$ averaged over 5000 particles versus time. To see this figure in color, go online.

opposite case, when the amount of F-actin is large, the active stress is saturated and a stable, uniform, high-tension state is maintained despite any small nonuniformities in F-actin density. Such F-actin-rich structures include the lamellipodial protrusions of migrating cells (e.g., in the keratocytes described in Barnhart et al. (18)) and the apical ZA of epithelial cells. The latter case is consistent with our earlier observation that F-actin stabilization enhances tension at the ZA. Interestingly, we have also found that stimulating myosin II by expressing a phosphomimetic regulatory light chain increases tension at the ZA to only a limited extent (26), suggesting that stress at the actin-rich ZA may be close to saturation.

However, at intermediate F-actin concentrations, small nonuniformities in the concentration are self-amplified by the contractile flow they generate and produce persistent condensation centers. Thus, in this regime the contractile medium tears itself apart and produces a nonuniform concentration field and tension distribution. In these spatial structures, the actomyosin cortex may condense into static spots or stripes similar to the well-known Turing patterns at intermediate *Pe*. At larger *Pe*, the system typically produces a persistent dynamic behavior with a continuous cycle of high-concentration clusters forming and merging. Furthermore, in the case of stress-dependent decay of F-actin, the highly condensed spot-like clusters are suppressed, allowing the formation of a dynamically changing actin network in a certain range of parameters. This is qualitatively similar to the behavior observed on the lateral cortex in epithelial cell sheets, where F-actin stability is lower than that found at the ZA (23). Furthermore, we found that reducing F-actin stability at the ZA caused apical cadherin clusters to convert from stationary motion to oscillatory movements, which is identical to what was seen at the lateral junctions. In our model, this would be equivalent to moving from a high F-actin concentration regime to an intermediate concentration regime.

Our results establish that F-actin turnover can function as an important regulator of pattern formation and dynamics in a theoretical model of the actomyosin cortex. This has the potential to influence the mechanical properties of the interactions between epithelial cells. We considered a simple model that neglected the polar nature of the contractile system composed of actin filaments and the elastic properties of the medium. Formally, this model is applicable to many biological situations that are distinguished by an actomyosin-rich cortex. In addition, we have not yet considered the potential contribution of E-cadherin adhesion, which may influence cortical dynamics at junctions in at least two ways. First, coupling of F-actin to cadherin adhesion may represent a source of friction on the contractile cortex, which may be further amplified as adhesion allows mechanical coupling to the cortex of the neighboring cells. Second, the E-cadherin system promotes actin assembly and myosin activation to facilitate biogenesis of the contractile junctional cortex itself. Extending the model to take into account these additional complexities in further work may allow for a more accurate quantitative representation of actomyosin patterns on the cortex as they are modified by interactions with other cells.

SUPPORTING MATERIAL

Six movies are available at http://www.biophysj.org/biophysj/supplemental/S0006-3495(14)01131-X.

This work was supported by the National Health and Medical Research Council of Australia (1037320, 1044041, and 1067405), the Australian Research Council (DP120104667 and FT130100659), and the Kids Cancer Project of the Oncology Research Foundation. Confocal microscopy was performed at the ARCF/IMB Cancer Biology Imaging Centre established with the generous support of the Australian Cancer Research Foundation.

REFERENCES

1. Turing, A. 1952. The chemical basis of morphogenesis. *Philos. Trans. R. Soc. Lond. B Biol. Sci.* 237:37–72.
2. Gierer, A., and H. Meinhardt. 1972. A theory of biological pattern formation. *Kybernetik.* 12:30–39.
3. Kondo, S., and T. Miura. 2010. Reaction-diffusion model as a framework for understanding biological pattern formation. *Science.* 329: 1616–1620.
4. Sheth, R., L. Marcon, …, M. A. Ros. 2012. Hox genes regulate digit patterning by controlling the wavelength of a Turing-type mechanism. *Science.* 338:1476–1480.
5. Sick, S., S. Reinker, …, T. Schlake. 2006. WNT and DKK determine hair follicle spacing through a reaction-diffusion mechanism. *Science.* 314:1447–1450.
6. Mori, Y., A. Jilkine, and L. Edelstein-Keshet. 2008. Wave-pinning and cell polarity from a bistable reaction-diffusion system. *Biophys. J.* 94:3684–3697.
7. Kholodenko, B. N. 2006. Cell-signalling dynamics in time and space. *Nat. Rev. Mol. Cell Biol.* 7:165–176.
8. Munoz-Garcia, J., Z. Neufeld, and B. N. Kholodenko. 2009. Positional information generated by spatially distributed signaling cascades. *PLoS Comput. Biol.* 5:e1000330.
9. Csikász-Nagy, A., B. Gyorffy, …, B. Novák. 2008. Spatial controls for growth zone formation during the fission yeast cell cycle. *Yeast.* 25:59–69.
10. Howard, J., S. W. Grill, and J. S. Bois. 2011. Turing's next steps: the mechanochemical basis of morphogenesis. *Nat. Rev. Mol. Cell Biol.* 12:392–398.
11. Tee, S.-Y., A. R. Bausch, and P. A. Janmey. 2009. The mechanical cell. *Curr. Biol.* 19:R745–R748.
12. Rauzi, M., P. Verant, …, P.-F. Lenne. 2008. Nature and anisotropy of cortical forces orienting *Drosophila* tissue morphogenesis. *Nat. Cell Biol.* 10:1401–1410.
13. Goehring, N. W., and S. W. Grill. 2013. Cell polarity: mechanochemical patterning. *Trends Cell Biol.* 23:72–80.
14. Fletcher, D. A., and R. D. Mullins. 2010. Cell mechanics and the cytoskeleton. *Nature.* 463:485–492.
15. Joanny, J.-F., and J. Prost. 2009. Active gels as a description of the actin-myosin cytoskeleton. *HFSP J.* 3:94–104.
16. Banerjee, S., and M. Marchetti. 2010. Instabilities and oscillations in isotropic active gels. *Soft Matter.* 7:463–473.
17. Rubinstein, B., M. F. Fournier, …, A. Mogilner. 2009. Actin-myosin viscoelastic flow in the keratocyte lamellipod. *Biophys. J.* 97:1853–1863.
18. Barnhart, E. L., K. C. Lee, …, J. A. Theriot. 2011. An adhesion-dependent switch between mechanisms that determine motile cell shape. *PLoS Biol.* 9:e1001059.
19. Ben Isaac, E., U. Manor, …, N. S. Gov. 2013. Linking actin networks and cell membrane via a reaction-diffusion-elastic description of nonlinear filopodia initiation. *Phys. Rev. E Stat. Nonlin. Soft Matter Phys.* 88:022718.
20. Salbreux, G., J. Prost, and J. F. Joanny. 2009. Hydrodynamics of cellular cortical flows and the formation of contractile rings. *Phys. Rev. Lett.* 103:058102.
21. Weiner, O. D., W. A. Marganski, …, M. W. Kirschner. 2007. An actin-based wave generator organizes cell motility. *PLoS Biol.* 5:e221.
22. Graziano, B. R., and O. D. Weiner. 2014. Self-organization of protrusions and polarity during eukaryotic chemotaxis. *Curr. Opin. Cell Biol.* 30C:60–67.
23. Wu, S. K., G. A. Gomez, …, A. S. Yap. 2014. Cortical F-actin stabilization generates apical-lateral patterns of junctional contractility that integrate cells into epithelia. *Nat. Cell Biol.* 16:167–178.
24. Bois, J. S., F. Jülicher, and S. W. Grill. 2011. Pattern formation in active fluids. *Phys. Rev. Lett.* 106:028103.
25. Burkel, B. M., G. von Dassow, and W. M. Bement. 2007. Versatile fluorescent probes for actin filaments based on the actin-binding domain of utrophin. *Cell Motil. Cytoskeleton.* 64:822–832. http://dx.doi.org/10.1002/cm.20226.
26. Taylor, Z. J., R. Gurka, G. A. Kopp, and A. Liberzon. 2010. Long-duration time-resolved PIV to study unsteady aerodynamics. *IEEE Trans. Instrum. Meas.* 59:3262–3269.
27. Wu, S. K., S. Budnar, …, G. A. Gomez. 2014. Pulsatile contractility of actomyosin networks organizes the cellular cortex at lateral cadherin junctions. *Eur. J. Cell Biol.*: pii:S0171-9335(14)00108-3.
28. Kovacs, E. M., S. Verma, …, A. S. Yap. 2011. N-WASP regulates the epithelial junctional actin cytoskeleton through a non-canonical post-nucleation pathway. *Nat. Cell Biol.* 13:934–943.
29. Kumar, K. V., J. S. Bois, …, S. W. Grill. 2014. Pulsatory patterns in active fluids. *Phys. Rev. Lett.* 112:208101.
30. Leerberg, J. M., G. A. Gomez, …, A. S. Yap. 2014. Tension-sensitive actin assembly supports contractility at the epithelial zonula adherens. *Curr. Biol.* 24:1689–1699.